ACSNANO
www.acsnano.org
ARTICLE

Color-Tunable Resonant Photoluminescence and Cavity-Mediated Multistep Energy Transfer Cascade

Daichi Okada,[†] Takashi Nakamura,[‡] Daniel Braam,[§] Thang Duy Dao,[∥,⊥] Satoshi Ishii,[∥,⊥] Tadaaki Nagao,[∥,⊥] Axel Lorke,[§] Tatsuya Nabeshima,[‡,¶,#] and Yohei Yamamoto*[,†,¶,#]

[†]Division of Materials Science, Faculty of Pure and Applied Sciences, University of Tsukuba, 1-1-1 Tennodai, Tsukuba, Ibaraki 305-8573, Japan

[‡]Division of Chemistry, Faculty of Pure and Applied Sciences, University of Tsukuba, 1-1-1 Tennodai, Tsukuba, Ibaraki 305-8571, Japan

[§]Faculty of Physics and CENIDE, University of Duisburg—Essen, Lotharstrasse 1, Duisburg D-47048, Germany

[∥]International Center for Materials Nanoarchitectonics (WPI-MANA), National Institute for Materials Science (NIMS), 1-1 Namiki, Tsukuba, Ibaraki 305-0044, Japan

[⊥]CREST, Japan Science and Technology Agency (JST), 4-1-8 Honcho, Kawaguchi, Saitama 332-0012, Japan

[¶]Tsukuba Research Center for Interdisciplinary Materials Science (TIMS), Faculty of Pure and Applied Sciences, University of Tsukuba, 1-1-1 Tennodai, Tsukuba, Ibaraki 305-8571, Japan

[#]Center for Integrated Research in Fundamental Science and Technology (CiRfSE), University of Tsukuba, 1-1-1 Tennodai, Tsukuba, Ibaraki 305-8571, Japan

S *Supporting Information*

ABSTRACT: **Color-tunable resonant photoluminescence (PL) was attained from polystyrene microspheres doped with a single polymorphic fluorescent dye, boron-dipyrrin (BODIPY) 1. The color of the resonant PL depends on the assembling morphology of 1 in the microspheres, which can be selectively controlled from green to red by the initial concentration of 1 in the preparation process of the microspheres. Studies on intersphere PL propagation with multicoupled microspheres, prepared by micromanipulation technique, revealed that multistep photon transfer takes place through the microspheres, accompanying energy transfer cascade with stepwise PL color change. The intersphere energy transfer cascade is direction selective, where energy donor-to-acceptor down conversion direction is only allowed. Such cavity-mediated long-distance and multistep energy transfer will be advantageous for polymer photonics device application.**

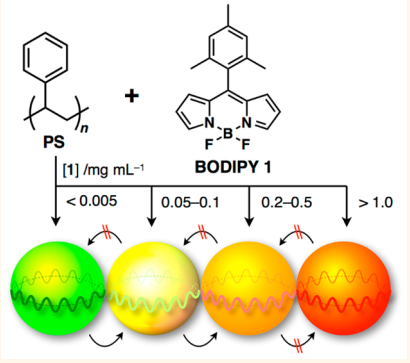

KEYWORDS: *BODIPY, microsphere, energy transfer, whispering gallery mode, photoluminescence*

Energy transfer plays an important role in natural and artificial photosynthesis systems[1−5] and optoelectronic devices,[6,7] in which light energy is harvested and converted into chemical and electric energies. Energy transfer often accompanies down-conversion of photons with the directional energy flow from energy donor to acceptor. In general, energy transfer processes are categorized into two mechanisms. One is radiative energy transfer, where photoluminescence (PL) from one fluorophore is reabsorbed by a different chromophore that emits PL with different energy.[8] Radiative energy transfer occurs at long-range, but the efficiency per unit volume is quite low because of the dispersion of radiation. The other mechanism of energy transfer is nonradiative process such as fluorescence resonance energy transfer (FRET).[5,7−9] In the nonradiative process, the efficiency of energy transfer is high, but the effective distance is short within only less than ten nanometers. Therefore, one of promising ways to attain energy transfer at long-range with high efficiency is to guide PL directionally from the energy-donating fluorophore to the energy-accepting fluorophore.

In this article, we demonstrate long-range energy transfer and its cascade by using polymorphic dye-doped polystyrene (PS) microspheres. The dye we used was boron-dipyrrin (BODIPY)

Received: May 13, 2016
Accepted: June 27, 2016
Published: June 27, 2016

DOI: 10.1021/acsnano.6b03188
ACS Nano 2016, 10, 7058−7063

derivative **1**.[10,11] Typically, the BODIPY frame emits green PL in a diluted solution.[10−13] The PL color varies with the molecular structure and aggregated state of BODIPY.[14,15] We found that the **1**-doped PS microspheres exhibit resonant PL with various colors from green to red that depends on the polymorph of **1**, which can be controlled by the initial concentration of **1** in the self-assembling process. Furthermore, the connection of the **1**-doped PS microspheres results in cavity-mediated long-range FRET at ranges as long as several micrometers. The energy transfer cascade occurs through two-to-four coupled microspheres, where the photon transfer occurs in a selective direction. The long-distance, direction-selective photon transfer will be advantageous for fully polymeric optical circuits.

RESULTS AND DISCUSSION

Preparation and PL Properties of Polymorphic BODIPY-Doped PS Microspheres. The molecular structure of **1** is drawn in Figure 1a. The wavelengths of photoabsorption and PL maxima (λ_{abs} and λ_{em}, respectively) of **1** in $CHCl_3$ are 503 and 517 nm, respectively, (Figure S1) with a fluorescence quantum yield (ϕ_{PL}) of 0.88 in solution. The **1**-doped PS microspheres were fabricated by the interface precipitation method in an open system (Figure 1a, inset; for details, see Experimental Section and Figure S2). Scanning electron microscopy (SEM) images of the air-dried suspensions show well-defined microspheres (Figure 1b−e, inset) with the average diameters (d_{av}) of 2.4−4.4 μm (Figure S3a−d). Both d_{av} values and its standard deviation (σ) decrease when the fraction of EtOH in the nonsolvent increased (Figure S3e−i).

Fluorescent microscopy (FM) observations indicate that the PL color of the microspheres varies systematically with the initial concentration of **1**, and the microspheres prepared in the same batch show a homogeneous fluorescent color: Microspheres prepared from tetrahydrofuran (THF) solution at [**1**] = 0.005 mg mL^{-1} displayed green PL (Figure 1b). As [**1**] increased to 0.1, 0.5, and 1.0 mg mL^{-1}, the resultant microspheres displayed PL with yellow, orange, and red colors, respectively (Figure 1c−e). For comparison, when the vial was capped during the self-assembly process (closed system), the precipitation was not completed even after 12 h (Figure S4a−f), and the fluorescent color of the resultant microspheres was not homogeneous but varied within a single batch (Figure S4g−k). Therefore, rapid precipitation in an open system is appropriate for preparing microspheres that exhibit PL with selected colors.

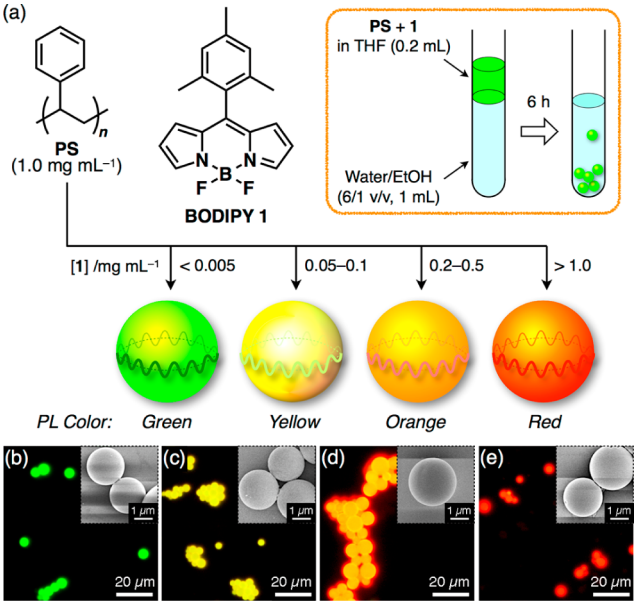

Figure 1. (a) Schematic representation of the formation of PS microspheres with multicolor resonant PL with different doping levels of 1 prepared by interface precipitation method. (b−e) FM images of PS microspheres with different doping levels of 1. Initial concentrations of 1 are 0.005 (b), 0.1 (c), 0.5 (d), and 1.0 mg mL^{-1} (e). λ_{ex} = 400−440 nm (stationary light). Insets show SEM images of the corresponding microspheres.

PL spectra of cast films of the resultant microspheres show a systematic change of the PL bands with the initial concentration of **1** (Figure 2a). Microspheres prepared with

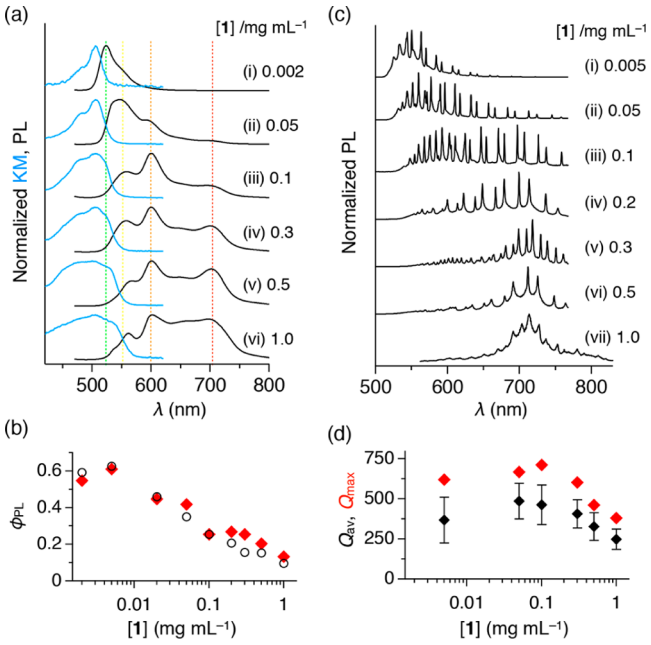

Figure 2. (a) Normalized Kubelka−Munk (KM, blue) and PL (black) spectra of cast films of PS microspheres prepared at different [1]. λ_{ex} = 450 nm (stationary light). (b) Plots of ϕ_{PL} of cast films of PS microspheres (red squares) and those prepared from PS solution (black circles) versus [1]. λ_{ex} = 450 nm (stationary light). (c) μ-PL spectra of a single PS microsphere prepared at different [1]. λ_{ex} = 470 nm (focused laser). The values on the right side of the spectra indicate initial [1] in the preparation process. (d) Plots of average (black) and maximum (red) Q factors (Q_{av} and Q_{max}, respectively) versus [1]. For calculation of Q_{av}, 45−93 WGM PL lines from 5−7 microspheres (d = 3.1−8.1 μm) were used (error bars: the standard deviation).

[**1**] = 0.002 mg mL^{-1} showed PL with λ_{em} = 523 nm (Figure 2a(i)), which almost coincides with the PL spectrum of **1** in $CHCl_3$ (Figure S1). This result indicates that **1** is molecularly dispersed in the PS matrix. When [**1**] increased to 0.05 mg mL^{-1}, λ_{em} shifted to 547 nm (Figure 2a(ii)), originating from the amorphous aggregates of **1** (Figure S5). In addition, a weak shoulder band appeared at 600 nm in the PL spectrum, which derives from the excimer emission from J-aggregated **1**.[15] Further increase of [**1**] to 0.1 mg mL^{-1} enhanced the PL peak at 600 nm, accompanied by a new PL band at 700 nm (Figure 2a(iii)). The intensity of the PL band at 700 nm increased as

DOI: 10.1021/acsnano.6b03188
ACS Nano 2016, 10, 7058−7063

[**1**] increased to 0.3 and 0.5 mg mL^{-1} (Figure 2a(iv) and (v)) and became comparable to that at 600 nm when [**1**] reached 1.0 mg mL^{-1} (Figure 2a(vi)). The PL at 700 nm possibly originates from the modulation of the reflection by a crystalline habit of **1** in the PS microsphere.[15] Concomitantly, as [**1**] increased, the absorption edge shifted from 525 to 560 nm (Figure 2a, blue). Because ϕ_{PL} of the microspheres coincides well with that of thin films prepared by drop-cast solutions of PS and **1** (Figure 2b), the doping level of **1** in the microspheres is considered nearly identical to the initial weight ratio of **1** to PS. A concentration quenching causes a drop of ϕ_{PL} upon increasing [**1**] (Figure 2b).

Resonant PL from BODIPY-Doped Single Microsphere. PL spectra of a single microsphere were measured by the μ-PL technique under an ambient condition by focused laser excitation on the perimeter of the microspheres (λ_{ex} = 470 nm, spot size ~0.5 μm, see Experimental Section and Figure S6).[16−19] Each microsphere exhibited sharp and periodic PL lines superimposing on the broad PL band (Figure 2c). The sharp PL lines derive from the whispering gallery mode (WGM) caused by the confinement via total internal reflection at the polymer−air interface.[16−22] The resonance occurs when the wavelength of the PL is an integer multiple of the circumference of the microspheres. The sharp and periodic peaks are identified as transverse electric (TE) and magnetic (TM) modes, which are indexed in Figure S7.[23] As the diameter (d) of the microspheres increases, the spacing between the WGMs decreases because of the longer optical path around the microspheres' circumference.

The observed PL wavelength range and Q-factor of the WGM PL lines depend on the doping level of **1**. The microspheres prepared at [**1**] = 0.005 mg mL^{-1} displayed strong WGM PL peaks at 520−600 nm (Figure 2c(i)), which roughly coincides with the wavelength region observed from PL spectra of the cast film of the corresponding microspheres (Figure 2a(i)). For microspheres prepared at [**1**] = 0.05 mg mL^{-1}, intense WGM lines appeared at 550−600 nm, and weak lines were observed up to 750 nm (Figure 2c(ii)). Further increase of [**1**] to 0.1 mg mL^{-1} resulted in the intense WGM lines with a wide wavelength region at 550−750 nm (Figure 2c(iii)). When [**1**] was higher than 0.3, the WGM lines were mainly observed at 700−750 nm (Figure 2c(v)−(vii)), which is in contrast with the PL spectra of cast films of the microspheres, where a broad PL band appeared at 550−750 nm (Figure 2a(iv)−(vi)). In the case of μ-PL, the confined PL in the short wavelength region tends to be reabsorbed efficiently, and thus WGM lines appeared only in the long wavelength region. It is worth noting that Q-factors, defined by the wavelength of a PL peak divided by the full width at half-maximum, decreased when [**1**] increased above 0.1 mg mL^{-1} (Figures 2d and S8), which possibly resulted from the Rayleigh scattering by crystalline nanodomains of **1** in the microspheres.

Cavity-Mediated Intersphere Energy Transfer in Bispheres. We conducted intersphere propagation and color conversion of the confined PL using coupled microspheres. Hereafter, microspheres with green, yellow, orange, and red PL are abbreviated as **G**, **Y**, **O**, and **R**, respectively. First, two microspheres with the identical PL color were coupled (**G**−**G**, **Y**−**Y**, **O**−**O**, and **R**−**R**), and the perimeter of one side of the bisphere was photoexcited by a focused laser beam. For the bisphere of **G**−**G**, green PL was observed at the excitation point, contact point, and even at the opposite side to the contact point (Figure S9a). On the basis of the cross-section profile of the FM images upon focused laser excitation, we evaluate the average ratio of the PL transfer (r) as

$$r = \frac{I_{PL2}}{I_{PL1}} \quad (1)$$

where I_{PL1} and I_{PL2} represent the gray value of the PL intensity from the position of the photoexcitation and that opposite to the connected point of the adjacent microsphere, respectively (Figure S9a bottom). The $r_{G\rightarrow G}$ value is evaluated as 0.58. On the other hand, in the case of **Y**−**Y**, **O**−**O**, and **R**−**R**, the ratio is smaller with $r_{Y\rightarrow Y}$, $r_{O\rightarrow O}$, and $r_{R\rightarrow R}$ of 0.50, 0.25, and 0.26, respectively (Figure S9b−d). In general, intersphere propagation of WGM is not efficient because the peak positions are not identical owing to the size mismatch of the spheres.

Next, PL transfer of coupled microspheres with different PL properties was investigated. When **G** and **Y** were in contact, and the perimeter of **G** was excited, green PL was observed from **G**, whereas yellow PL was observed from **Y** (Figure 3a). This result indicates that the green PL generated inside **G** propagates along the circumference, which is reabsorbed by **Y** at the contact point, and then **Y** emits the yellow PL. Judging from the cross section PL intensity profile, the yellow PL from **Y** is of similar intensity or even stronger than the green PL from **G** (Figure 3a, bottom). The $r_{G\rightarrow Y}$ value is evaluated as 1.00, which is much higher than $r_{G\rightarrow G}$ (0.58). In contrast, upon excitation at **Y**, yellow PL was observed from both **Y** and **G**, but the PL intensity from **G** was very weak (Figure 3b). The cross section profile shows that the PL intensity is largely decreased after propagation to **G** with the $r_{Y\rightarrow G}$ value of 0.39 (Figure 3b, bottom).

We found that PL from the adjacent microsphere involves WGM after the color conversion. Upon excitation at **G** of the bisphere of **G**−**Y**, the WGM character from **G** was less pronounced (Figure 3c, black) than that from the isolated **G** (Figure 2c(i)). In contrast, the PL spectrum from the adjacent **Y** showed a clear WGM fingerprint (Figure 3c, red), which is almost identical as that from **Y** upon excitation at **Y** (Figure 3d, black). Note that, upon excitation at **Y**, yellow WGM PL was observed from **G** without wavelength conversion (Figure 3d, red), though the PL intensity became very weak after propagation.

The asymmetric photon transfer behavior (i. e., $r_{G\rightarrow Y} > r_{Y\rightarrow G}$) was also observed from the coupled **G**−**O** (Figure S10a and b) and **G**−**R** (Figure S10c and d). The average PL intensity ratios, $r_{G\rightarrow O}$ and $r_{G\rightarrow R}$, are 1.02 and 0.79, respectively, whereas those of the reverse direction, $r_{O\rightarrow G}$ and $r_{R\rightarrow G}$, are only 0.16 and 0.18, respectively. The degree of the asymmetric photon transfer, expressed as $r_{G\rightarrow X}/r_{X\rightarrow G}$ (**X** = **Y**, **O**, and **R**), is evaluated to be in the range of 2.5−6.4. On the other hand, combinations of the bispheres such as **Y**−**O**, **Y**−**R**, and **O**−**R** displayed rather small r values (<0.5) for both forward and reverse directions, and the degrees of asymmetric photon transfer are only within 1.0−2.1 (Figure S10e−j). One reason is referred to the energy transfer efficiency; PL from **G** (λ_{em} = 523 nm, Figure 2a(i)) largely overlaps with the photoabsorption bands of **Y**, **O**, and **R** (Figure 2a(iii)−(vi) blue), and thereby the excitation energy in **G** is transferrable to **Y**, **O**, and **R**. On the other hand, the Stokes shift in **Y** and **O** is large in comparison with that of **G**, which causes small overlap with the absorption bands of **O** and **R** (Figure 2a(v)−(vi)), leading to low efficiencies of **Y**-to-**O**, **Y**-to-**R**, and **O**-to-**R** energy transfer. The WGM spectral change was observed for the bisphere of **G**−**O** (Figure S11a and b) and **Y**−

DOI: 10.1021/acsnano.6b03188
ACS Nano 2016, 10, 7058−7063

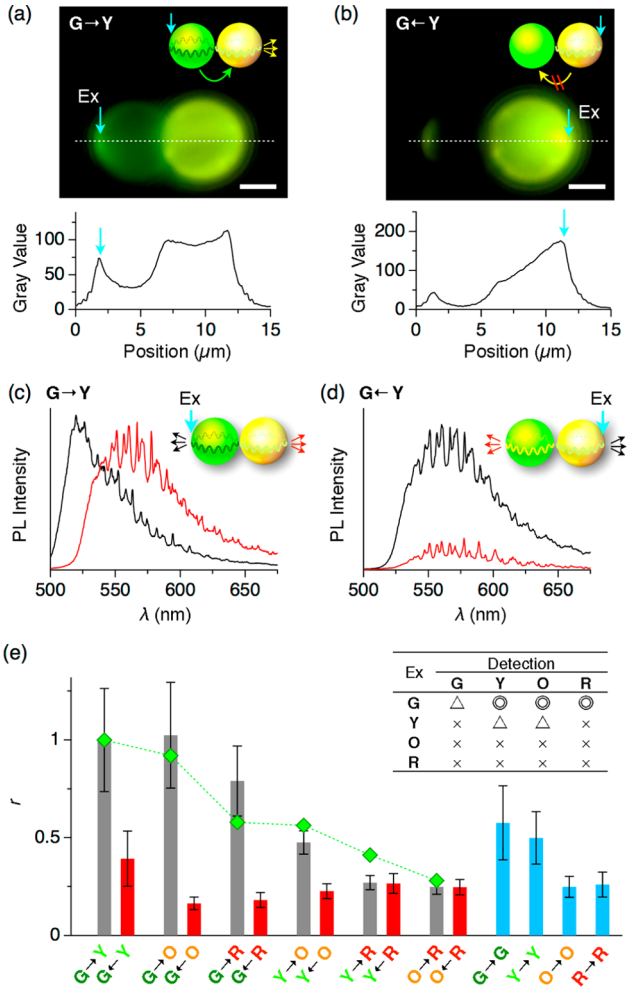

Figure 3. (a, b) FM images of a bisphere of G−Y upon focused laser excitation (λ_{ex} = 470 nm) at the perimeters of one sphere (blue arrow). The bottom graphs show cross-section profiles of the PL intensities. Scale bars: 3 μm. (c, d) PL spectra of a bisphere of G−Y upon focused laser excitation (λ_{ex} = 405 nm) at G (c) and Y (d). The black and red spectra indicate PL at the excitation position and that from the adjacent microsphere, respectively. (e) Bar chart of the average ratio of the PL intensity (r) for bispheres. Each value is evaluated from measurements of 8−20 bispheres (error bars: the standard deviation). The data are listed in Table S1. The green plot shows relative values of the product of the area of the spectral overlap A and ϕ_{PL} of the energy-accepting microspheres. Inset shows table of the degree of r: ◎, r > 0.75; △, 0.45 < r < 0.6; ×, r < 0.4.

O (Figure S11c and d), yet in the latter case, the PL intensity after propagation became very small because of the low energy transfer efficiency. Note that, according to the results on an excitation of bispheres of coupled nondoped and doped PS microspheres, the influence of the direct excitation of the adjacent sphere by the propagation of the laser beam is negligible. Upon laser irradiation to the nondoped PS microsphere, PL from the adjacent **G**, **Y**, and **O** were very weak in comparison with PL by the excitation of the **1**-doped microspheres (Figure S12).

Figure 3e shows a bar chart of r for the bispheres with all combinations. The r values, listed in Table S1, are high for **G**-to-**Y**, **G**-to-**O**, and **G**-to-**R** in comparison with the bispheres with the opposite direction and the other combinations. As plotted in Figure 3e (green squares), the tendency of r for the intersphere donor-to-acceptor energy transfer can be qualitatively reproduced by numerical calculation of a product of two parameters: the area (A) of the spectral overlap between PL of energy-donating spheres and photoabsorption of energy-accepting spheres (Figure S13) and ϕ_{PL} of the energy-accepting spheres (Figure 2b).

Direction-selective, Long-Range Energy Transfer Cascade with Multicoupled Microspheres. The direction-selective PL transfer was clearly observed using a triple sphere arrangement. For connecting microspheres with different PL colors, we used a micromanipulation technique with an electrically controlled stepping stage and a thin microneedle. For a linearly connected **G**, **G**, and **O** (**G**−**G**−**O**), excitation at the central **G** resulted in the selective **G**-to-**O** PL transfer (Figure 4a). The cross section profiles of the PL intensity show that $r_{G\rightarrow O}$ is 1.2−1.7, whereas $r_{G\rightarrow G}$ is only ∼0.27 (Figure 4a, bottom). This result clearly indicates that PL transfer occurs selectively in the energy-transferrable direction. As expected

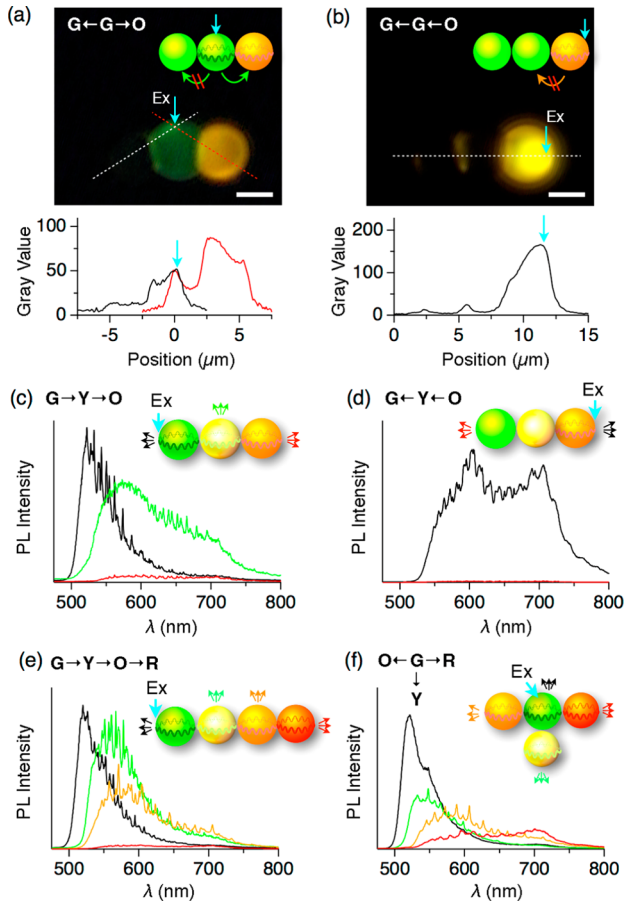

Figure 4. (a, b) FM images of coupled three spheres of G−G−O upon focused laser excitation (λ_{ex} = 470 nm) at the central G (a) and O (b). The bottom graphs show cross section profiles of the PL intensities. (c, d) PL spectra of coupled three spheres of G−Y−O upon focused laser excitation (λ_{ex} = 405 nm) at G (c) and O (d). The black, green, and red spectra indicate PL at the excitation position and that from the center and the opposite side, respectively. Insets show schematic illustrations of the coupled three spheres. (e, f) PL spectra of coupled four spheres of G, Y, O, and R with linear (e) and T-shaped (f) configurations upon focused laser excitation at G (λ_{ex} = 405 nm). The black, green, orange, and red spectra indicate PL from G, Y, O, and R, respectively. Insets show schematic illustrations of the coupled four spheres.

DOI: 10.1021/acsnano.6b03188
ACS Nano 2016, 10, 7058−7063

from the bisphere experiments, excitation at **O** hardly transferred PL to the adjacent **G** ($r_{O\rightarrow G}$ = 0.15, Figure 4b).

Multistep energy transfer cascade was found for triply connected microspheres with linearly connected **G**, **Y**, and **O** (**G**−**Y**−**O**). Upon laser excitation of **G**, stepwise **G**-to-**Y** and **Y**-to-**O** energy transfer occurs, yet the transfer efficiency of the latter is smaller than that of the former (Figure 4c). However, the WGM character was still observed after the PL transfer, along with a certain red shift of the PL spectra (Figure S14a). The PL transfer in the opposite direction was very poor (Figure 4d). Similarly, energy cascade and PL spectral shift were observed for four microspheres of **G**, **Y**, **O**, and **R** with linear and T-shaped configuration (Figure 4e and f, respectively) while involving the WGM character corresponding to each microsphere (Figure S14c, d).

CONCLUSIONS

In summary, single polymorphic dye-doped polystyrene microspheres display whispering gallery mode (WGM) resonant photoluminescence with multiple colors from green to red. The coupled bispheres show cavity-mediated long-range energy transfer, where confined photons transfer only one way from the energy-donating sphere to the energy-accepting sphere. The multicoupled microspheres exhibit cascading energy transfer, accompanying the multistep color conversion while maintaining the WGM character even after the transfer. The reciprocal transfer of photons on the micrometer scale will be advantageous for applications to compact optical integrated devices.

EXPERIMENTAL SECTION

General. Unless otherwise noted, reagents and solvents were used as received from Sigma-Aldrich Co. LLC, Tokyo Chemical Industry Co. Ltd. and Nakarai Tesque Co. Polystyrene (PS) was purchased from Sigma-Aldrich Co. LLC (weight-average molecular weight M_w = 35 000). The *N*,*N*′-difluoroboryl-5-mesityldipyrrin (BODIPY) **1** was synthesized according to the reported procedures.[10] Photoabsorption spectra were recorded on a JASCO V-570 spectrophotometer, and diffuse reflectance spectra were recorded on the same apparatus equipped with a JASCO model ISN-470 integrating sphere option. Fluorescence spectra were recorded on a JASCO FP-8300 spectrofluorometer. Fluorescence quantum yield (ϕ_{PL}) was recorded on a Hamamatsu model C9920−02 absolute PL quantum yield measurement system. SEM was performed on a Hitachi model SU-8020 FE-SEM and JEOL model JSM-5610 SEM operating at 10 and 20 kV, respectively. Silicon was used as a substrate and Au for coating. Optical and fluorescent microscope observation was carried out using an Olympus model BX53 Upright Microscope. For the fluorescent microscopy observation with stationary light excitation, the excitation light with wavelength λ_{ex} = 400−440 nm was used, and long-pass filter (>460 nm) was used for the detection of the images. Powder X-ray diffraction (PXRD) patterns were recorded at 25 °C on RIGAKU model Miniflex600 with a Cu*Kα* radiation source (40 kV and 15 mA).

Preparation of 1-Doped PS Microspheres. The **1**-doped PS microspheres were prepared by interface precipitation method (Figure 1a, inset). Typically, a THF solution of a mixture of PS ([PS] = 1.0 mg mL^{-1}) and **1** ([**1**] = 0.002−1.0 mg mL^{-1} = 6.4−3200 μM) was carefully added onto a nonsolvent layer of a water/EtOH mixture (6/1 v/v, 1 mL). A slow diffusion of the solvents, along with simultaneous evaporation of THF to air, resulted in a precipitation after 6 h of aging.

***μ*-PL Measurements.** *μ*-PL measurements of single microspheres were carried out using a *μ*-PL measurement system (Figure S6).[17] An optical microscope was used with a long-distance 100× objective (NA = 0.8) to identify suitable particles and determine their diameters (*d*). For measurements, a WITec *μ*-PL system was used with a model Alpha 300S microscope combined with a Princeton Instruments model Action SP2300 monochromator (grating: 300 grooves mm^{-1}) and an Andor iDus model DU-401A BR-DD-352 CCD camera cooled to −60 °C. The perimeter of a single microsphere was photoexcited at 25 °C under an ambient condition by a diode pulsed laser (a PicoQuant model LDH-D-C-470B with a PDL 828 "Sepia II" driver) with the wavelength, power, integration time, frequency, pulse duration, and spot size of 470 nm, 1.5 *μ*W, 0.1 s, 2.5 MHz, 70 ps, and ∼0.5 *μ*m, respectively.

For *μ*-PL measurements with different excitation and detection positions, the spheres were excited by a 405 nm Linos Nano-405-80 CW laser, and the light was collected within a confocal setup by a 50× objective with NA = 0.5 and detected by a 500 mm Acton SpectraPro 2500i spectrometer with a liquid-nitrogen-cooled CCD camera at −120 °C and a 150 grooves mm^{-1} grating.[19] Spot size, laser power, and integration time were 0.5 *μ*m, 0.5 *μ*W, and 1 s, respectively. To separate the detection spot from the excitation, the collimator optics of the excitation laser beam was tilted with respect to the optical axis of the detection path. In order to connect three and four microspheres, handmade micromanipulation apparatus with an electrically controlled stepping stage and a thin microneedle was used.

ASSOCIATED CONTENT

Supporting Information

The Supporting Information is available free of charge on the ACS Publications website at DOI: 10.1021/acsnano.6b03188.

Materials and measurements, sample preparation, UV−vis and PL spectra, XRD, WGM PL, and simulation. (PDF)

AUTHOR INFORMATION

Corresponding Author

*E-mail: yamamoto@ims.tsukuba.ac.jp.

Notes

The authors declare no competing financial interest.

ACKNOWLEDGMENTS

The authors acknowledge Prof. Akinori Saeki at Osaka University for PL measurements of the thin films. This work was partly supported by KAKENHI (25708020, 15H00860, 15H00986, 15K13812, 16H02081) from JSPS/MEXT, Japan, Asahi Glass Foundation, and University of Tsukuba-DAAD partnership program.

REFERENCES

(1) Barber, J.; Andersson, B. Revealing the Blueprint of Photosynthesis. *Nature* **1994**, *370*, 31−34.

(2) Li, X.; Sinks, L. E.; Rybtchinski, B.; Wasielewski, M. R. Ultrafast Aggregate-to-Aggregate Energy Transfer within Self-assembled Light-Harvesting Columns of Zinc Phthalocyanine Tetrakis-(Perylenediimide). *J. Am. Chem. Soc.* **2004**, *126*, 10810−10811.

(3) Ajayaghosh, A.; Praveen, V. K.; Vijayakumar, C.; George, S. J. Molecular Wire Encapsulated into *π*-Organogels: Efficient Supramolecular Light-Harvesting Antennae with Color-Tunable Emission. *Angew. Chem., Int. Ed.* **2007**, *46*, 6260−6265.

(4) Chen, L.; Honsho, Y.; Seki, S.; Jiang, D. Light-Harvesting Conjugated Microporous Polymers: Rapid and Highly Efficient Flow of Light Energy with a Porous Polyphenylene Framework as Antenna. *J. Am. Chem. Soc.* **2010**, *132*, 6742−6748.

(5) Zhang, C.; Zhao, J.; Wu, S.; Wang, Z.; Wu, W.; Ma, J.; Guo, S.; Huang, L. Intramolecular RET Enhanced Visible Light-Absorbing Bodipy Organic Triplet Photosensitizers and Application in Photooxidation and Triplet−Triplet Annihilation Upconversion. *J. Am. Chem. Soc.* **2013**, *135*, 10566−10578.

(6) Peumans, P.; Uchida, S.; Forrest, S. R. Efficient Bulk Heterojunction Photovoltaic Cells Using Small Molecular-Weight Organic Thin Films. *Nature* **2003**, *425*, 158−162.

DOI: 10.1021/acsnano.6b03188
ACS Nano 2016, 10, 7058−7063

(7) Xu, W.-L.; Wu, B.; Zheng, F.; Yang, X.-Y.; Jin, H.-D.; Zhu, F.; Hao, X.-T. Förster Resonance Energy Transfer and Energy Cascade in Broadband Photodetectors with Ternary Polymer Bulk Heterojunction. *J. Phys. Chem. C* **2015**, *119*, 21913−21920.
(8) Nguyen, H. M.; Seitz, O.; Peng, W.; Gartstein, Y. N.; Chabal, Y. J.; Malko, A. V. Efficient Radiative and Nonradiative Energy Transfer from Proximal CdSe/ZnS Nanocrystals into Silicon Nanomembranes. *ACS Nano* **2012**, *6*, 5574−5582.
(9) Belusáková, S.; Lang, K.; Bujdák, J. Hybrid Systems Based on Layered Silicate and Organic Dyes for Cascade Energy Transfer. *J. Phys. Chem. C* **2015**, *119*, 21784−21794.
(10) Kee, H. L.; Kirmaier, C.; Yu, L.; Thamyongkit, P.; Youngblood, W. J.; Calder, M. E.; Ramos, L.; Noll, B. C.; Bocian, D. F.; Scheidt, W. R.; Birge, R. R.; Lindsey, J. S.; Holten, D. Structural Control of the Photodynamics of Boron-Dipyrrin Complexes. *J. Phys. Chem. B* **2005**, *109*, 20433−20443.
(11) Hattori, S.; Ohkubo, K.; Urano, Y.; Sunahara, H.; Nagano, T.; Wada, Y.; Tkachenko, N. V.; Lemmetyinen, H.; Fukuzumi, S. Charge Separation in a Nonfluorescent Donor-Acceptor Dyad Derived from Boron Dipyrromethene Dye, Leading to Photocurrent Generation. *J. Phys. Chem. B* **2005**, *109*, 15368−15375.
(12) Loudet, A.; Burgess, K. BODIPY Dyes and Their Derivatives: Syntheses and Spectroscopic Properties. *Chem. Rev.* **2007**, *107*, 4891−4932.
(13) Ulrich, G.; Ziessel, R.; Harriman, A. The Chemistry of Fluorescent Bodipy Dyes: Versatility Unsurpassed. *Angew. Chem., Int. Ed.* **2008**, *47*, 1184−1201.
(14) Bonardi, L.; Kanaan, H.; Camerel, F.; Jolinat, P.; Retailleau, P.; Ziessel, R. Fine-Tuning of Yellow or Red Photo- and Electroluminescence of Functional Difluoro-boradiazaindacene Films. *Adv. Funct. Mater.* **2008**, *18*, 401−413.
(15) Spies, C.; Huynh, A.-M.; Huch, V.; Jung, G. Correlation between Crystal Habit and Luminescence Properties of 4,4-Difluoro-1,3-dimethyl-4-bora-3*a*,4*a*-diaza-*s*-indacene, An Asymmetric BODIPY Dye. *J. Phys. Chem. C* **2013**, *117*, 18163−18619.
(16) Tabata, K.; Braam, D.; Kushida, S.; Tong, L.; Kuwabara, J.; Kanbara, T.; Beckel, A.; Lorke, A.; Yamamoto, Y. Self-Assembled Conjugated Polymer Spheres as Fluorescent Microresonators. *Sci. Rep.* **2014**, *4*, 5902.
(17) Kushida, S.; Braam, D.; Pan, C.; Dao, T. D.; Tabata, K.; Sugiyasu, K.; Takeuchi, M.; Ishii, S.; Nagao, T.; Lorke, A.; Yamamoto, Y. Whispering Gallery Resonance from Self-Assembled Microspheres of Highly Fluorescent Isolated Conjugated Polymers. *Macromolecules* **2015**, *48*, 3928−3933.
(18) Braam, D.; Kushida, S.; Niemöller, R.; Prinz, G. M.; Saito, H.; Kanbara, T.; Kuwabara, J.; Yamamoto, Y.; Lorke, A. Optically Induced Mode Splitting in Self-Assembled, High Quality-Factor Conjugated Polymer Microcavities. *Sci. Rep.* **2016**, *6*, 19635.
(19) Kushida, S.; Braam, D.; Dao, T. D.; Saito, H.; Shibasaki, K.; Ishii, S.; Nagao, T.; Saeki, A.; Kuwabara, J.; Kanbara, T.; Kijima, M.; Lorke, A.; Yamamoto, Y. Conjugated Polymer Blend Microspheres for Efficient, Long-Range Light Energy Transfer. *ACS Nano* **2016**, *10*, 5543−5549.
(20) Humar, M.; Ravnik, M.; Pajk, S.; Musevic, I. Electrically Tunable Liquid Crystal Optical Microresonators. *Nat. Photonics* **2009**, *3*, 595−600.
(21) Ta, V. D.; Chen, R.; Sun, H. D. Tuning Whispering Gallery Mode Lasing from Self-Assembled Polymer Droplets. *Sci. Rep.* **2013**, *3*, 1362.
(22) Wei, C.; Liu, S.-Y.; Zou, C.-L.; Liu, Y.; Yao, J.; Zhao, Y. S. Controlled Self-Assembly of Organic Composite Microdisks for Efficient Output Coupling of Whispering-Gallery-Mode Lasers. *J. Am. Chem. Soc.* **2015**, *137*, 62−65.
(23) Oraevsky, A. N. Whispering-Gallery Waves. *Quantum Electron.* **2002**, *32*, 377−400.

DOI: 10.1021/acsnano.6b03188
ACS Nano 2016, 10, 7058−7063